

Low-frequency fluctuations in the magnetosheath near the magnetopause

Richard E. Denton,¹ S. Peter Gary,² Xinlin Li,¹ Brian J. Anderson,³ James W. LaBelle,¹ and Marc Lessard¹

Abstract. There are four low-frequency modes which may propagate in a high-beta nearly bi-Maxwellian plasma. These are the magnetosonic, Alfvén, ion acoustic, and mirror modes. This manuscript defines a procedure based on linear Vlasov theory for the unique identification of these modes by use of transport ratios, dimensionless ratios of the fluctuating field and plasma quantities. A single parameter, the mode deviation, is defined which characterizes the difference between the theoretical transport ratios of a particular mode and the observed ratios. The mode deviation is calculated using the plasma and magnetic field data gathered by the Active Magnetospheric Particle Tracer Explorers/Ion Release Module spacecraft to identify the modes observed in the terrestrial magnetosheath near the magnetopause. As well as determining the mode which best describes the observed fluctuations, it gives us a measure of whether or not the resulting identification is unique. Using 17 time periods temporally close to a magnetopause crossing, and confining our study to the frequency range from 0.01 to 0.04 Hz, we find that the only clearly identified mode in this frequency range is the mirror mode. Most commonly, the quasi-perpendicular mirror mode (with wave vector \mathbf{k} roughly perpendicular to the background magnetic field \mathbf{B}_0) is observed. In two events the quasi-parallel mirror mode ($\mathbf{k} \parallel \mathbf{B}_0$) was identified.

Introduction

The magnetized, collisionless plasmas of space can support a wide variety of modes which may propagate, damp, or grow. If such fluctuations attain a sufficiently enhanced level, they may modify the plasma properties, so understanding wave-particle interactions is fundamental to understanding the dynamics of many space plasmas. And the fundamental activity in understanding the consequences of any observed spectrum of enhanced magnetic fluctuations in a space plasma is to identify the mode or modes which contribute to that spectrum.

This manuscript defines a procedure for the identification of enhanced magnetic fluctuations at frequencies well below the proton cyclotron frequency in relatively homogeneous plasmas characterized by relatively isotropic ion distribution functions and applies this procedure to observations from the Active Magnetospheric

Particle Tracer Explorers/Ion Release Module (AMPTE/IRM) spacecraft in the terrestrial magnetosheath. A fundamental assumption of this work is that the appropriate theoretical model to describe the hot, tenuous plasmas of space is the Vlasov equation coupled to Maxwell's equations. This provides a more accurate description of wave properties than the MHD approximation used in some previously published research on low-frequency mode identification [Lacombe *et al.*, 1990; Song *et al.*, 1994]. Furthermore, it permits extension of the mode identification formalism to frequencies of the order of the proton cyclotron frequency and above. Recent studies by Krauss-Varban *et al.* [1994] and Orlowski *et al.* [1994] indicate that the kinetic description provides more accurate values for transport ratios than the Hall-MHD fluid model, and use of the fluid model can lead to incorrect conclusions about which dispersion surface the waves are on.

Another fundamental assumption of the work described here is that, for sufficiently weak fluctuations, linear theory is an appropriate tool for constructing identifiers of low-frequency plasma modes. If the magnetic fluctuations are of sufficiently large amplitude, that is, $|\delta B| \sim B_0$, where \mathbf{B}_0 represents the uniform background magnetic field, wave-wave interactions can be very strong and the concept of a normal mode propagating with well-defined properties may not be valid. However, for relatively weak fluctuations, that is, $|\delta B| \ll B_0$, wave-wave and wave-particle interactions

¹Physics and Astronomy Department, Dartmouth College, Hanover, New Hampshire.

²Los Alamos National Laboratory, Los Alamos, New Mexico.

³Applied Physics Laboratory, Johns Hopkins University, Laurel, Maryland.

are relatively weak and the linear theory construct of a weakly damped or growing mode with specific properties can provide a useful foundation for understanding the physics of the plasma system.

At frequency $f \ll F_{cp}$ where F_{cp} is the proton cyclotron frequency, up to four distinct modes can propagate in a relatively isotropic plasma: the three waves corresponding to the normal modes of MHD theory, and a fourth zero frequency mode. Identification of the three MHD modes in an isotropic plasma is impeded by the lack of a consistent nomenclature; they are often termed fast, intermediate, and slow, after their relative phase speeds at $\beta_{\parallel p} \ll 1$, where $\beta_{\parallel p} \equiv 8\pi n_p T_{\parallel p} / B_0^2$ is the proton parallel beta. However, at $\beta_{\parallel p} \gg 1$, the order of phase speeds is changed so that, for example, the properties of the mode with intermediate phase speed are quite different from those of the "intermediate" mode at low $\beta_{\parallel p}$. Because of this we prefer to use the terms ion acoustic, Alfvén, and magnetosonic based on the physical properties of the modes. In Table 1 we show the relative phase speeds of these modes for $\beta_{\parallel p} \ll 1$ and $\beta_{\parallel p} \gg 1$. The terms "quasi-parallel" and "quasi-perpendicular" (when referring to a mode) refer approximately to the regimes $5^\circ < \theta_{kB} \lesssim 30^\circ$ and $60^\circ \lesssim \theta_{kB} < 85^\circ$ where θ_{kB} represents the angle between the wave vector $\mathbf{k} = k_y \hat{\mathbf{y}} + k_z \hat{\mathbf{z}}$ and the background magnetic field $\mathbf{B}_0 = \hat{\mathbf{z}} B_0$. Krauss-Varban et al. [1994] have also recently concluded that the waves should be named in a way similar to that we have described. Our ion acoustic, Alfvén, and magnetosonic modes are the same as their "slow/sound," "Alfvén/ion cyclotron," and "fast/magnetosonic" modes.

Kinetic theory predicts the existence of a fourth zero frequency mode [Tajiri, 1967]. The ions of the terrestrial magnetosheath downstream of quasi-perpendicular shocks (shocks with interplanetary magnetic field roughly perpendicular to the bow shock normal) are usually observed to be anisotropic such that $T_{\perp} > T_{\parallel}$ where T_{\perp} and T_{\parallel} represent temperatures perpendicular and parallel to \mathbf{B}_0 [Tsurutani et al., 1982; Schopke et al., 1990; Anderson and Fuselier, 1993]. When the ions are sufficiently anisotropic, the zero frequency mode becomes the mirror instability [Tajiri, 1967].

The magnetic field fluctuations of the dayside terrestrial magnetosheath exhibit a wide variety of frequencies, amplitudes, and other properties. At frequencies approaching the proton gyrofrequency F_{cp} , typi-

cally of the order of 1 Hz, the largest amplitude fluctuations arise from the electromagnetic proton and He^{2+} cyclotron anisotropy instabilities [Gary et al., 1993]. These instabilities propagate on the Alfvén branch and have maximum growth rate at $\mathbf{k} \parallel \mathbf{B}_0$ [Denton et al., 1994]. A few simple identifiers such as frequency and magnetic compressibility [Schopke et al., 1990; Anderson et al., 1991] or polarization and propagation direction [Farris et al., 1993] have been used to distinguish the ion cyclotron instabilities from the mirror instability [McKean et al., 1992].

The largest amplitude fluctuations in the magnetosheath are often found at $f \lesssim 0.10$ Hz [Kaufmann et al., 1970; Crooker et al., 1979; Tsurutani et al., 1982; Mousaizis et al., 1986; Hubert et al., 1989a, b; Song et al., 1990, 1992, 1993; Lacombe et al., 1990, 1992], where the ion cyclotron modes are stable [Denton et al., 1994] and the mirror instability has a relatively small growth rate. (In some cases, ion cyclotron wave power at higher frequencies can dominate; see Anderson et al. [1994].) Fluctuations in this frequency regime may be due to a variety of sources, which include convection into the magnetosheath after excitation upstream of the bow shock [Engebretson et al., 1991] or at the bow shock [Gleaves and Southwood, 1991], inverse cascade of mode energy from shorter wavelength instabilities [e.g., Gary and Winske, 1993], excitation at the magnetopause and propagation into the sheath [Song et al., 1992], as well as from ion temperature anisotropy. The purpose of this manuscript is to provide a formalism for distinguishing among the four possible modes in the magnetosheath at such low frequencies. The method we describe, however, is a general one and can be applied to the identification of low-frequency fluctuations in any relatively homogeneous plasma in which the ion distributions are bi-Maxwellian in character with $T_{\perp i}/T_{\parallel i} \geq 1$.

Definition of Transport Ratios

Because of the diversity of sources, and the diversity of possible modes at low frequencies, a systematic approach is necessary to identify fluctuations at $f \leq 0.1$ Hz in the sheath. Gary and Winske [1992] and Gary [1992] introduced the term "transport ratios" to denote dimensionless ratios of the squares of fluctuating field and plasma quantities. These authors, as well as

Table 1. Relative Phase Speeds of Low-Frequency Modes in Isotropic Plasma for $\beta_{\parallel p} \ll 1$ and for $\beta_{\parallel p} \gg 1$

$\beta_{\parallel p}$	Relative Phase Speeds	Quasi-Parallel ($0^\circ < \theta_{kB} \lesssim 30^\circ$)	Quasi-Perpendicular ($60^\circ \lesssim \theta_{kB} < 90^\circ$)
$\ll 1$	slow intermediate fast	ion acoustic Alfvén magnetosonic	ion acoustic Alfvén magnetosonic
$\gg 1$	slow intermediate fast	Alfvén magnetosonic ion acoustic	Alfvén ion acoustic magnetosonic

Lacombe et al. [1990, 1992], *Belmont et al.* [1992], *Anderson et al.* [1994], and *Song et al.* [1994] have used different combinations of such ratios to identify low-frequency fluctuations in the magnetosheath. This manuscript addresses the same issue. However, we here attempt to be more complete than any of these previous efforts in that we use both plasma and magnetic field observations for our database, as well as Vlasov theory for the computation of the transport ratios. Our choice of identifiers is different from, but guided by the experience of, these previous publications. *Lacombe et al.* [1990, 1992] demonstrated the usefulness for identifying sheath modes of a quantity which indicates the phase relation between the density fluctuations and the fluctuations of the magnetic field parallel to \mathbf{B}_0 ; *Gary and Winske* [1992] and *Gary* [1992] showed the utility of the Alfvén ratio and the compressibility in the same domain, and *Song et al.* [1994] argued that an identifier based upon the component of fluctuating magnetic field parallel to \mathbf{B}_0 is also useful in the sheath.

Following *Gary and Winske* [1992], we will use the notation $\langle ab \rangle_{\mathbf{k}\omega}$ to indicate the correlation between a and b , which is a function of \mathbf{k} and ω . We estimate this quantity from the observed finite length discrete time series by first taking the discrete time Fourier transform of a and b and then computing the product $a_\omega b_\omega^*$, where b_ω^* is the complex conjugate of b_ω .

We base our identification procedure on the following transport ratios: the compressibility of the j th species [*Gary*, 1986]

$$C_j(\mathbf{k}, \omega) \equiv \frac{\langle \delta n_j \delta n_j \rangle_{\mathbf{k}\omega}}{n_j^2} \frac{B_0^2}{\langle \delta \mathbf{B} \cdot \delta \mathbf{B} \rangle_{\mathbf{k}\omega}}, \quad (1)$$

the Alfvén ratio of the j th species [*Matthaeus and Goldstein*, 1982]

$$R_{A,j}(\mathbf{k}, \omega) \equiv \frac{\langle \delta \mathbf{v}_j \cdot \delta \mathbf{v}_j \rangle_{\mathbf{k}\omega}}{V_A^2} \frac{B_0^2}{\langle \delta \mathbf{B} \cdot \delta \mathbf{B} \rangle_{\mathbf{k}\omega}}, \quad (2)$$

where $V_A \equiv B_0 / \sqrt{4\pi n_p m_p}$ is the Alfvén speed.

To these we add the parallel phase ratio

$$R_{\parallel n_j}(\mathbf{k}, \omega) \equiv \frac{\langle \delta n_j \delta B_{\parallel j} \rangle_{\mathbf{k}\omega}}{\sqrt{\langle \delta n_j \delta n_j \rangle_{\mathbf{k}\omega} \langle \delta B_{\parallel j} \delta B_{\parallel j} \rangle_{\mathbf{k}\omega}}}, \quad (3)$$

which is equivalent to the cosine of the phase angle between $\delta B_{\parallel j}$ and δn_j . This quantity is similar to the parallel compressibility of *Lacombe et al.* [1990] $C_{\parallel j}(\mathbf{k}, \omega) \equiv (\langle \delta n_j \delta B_{\parallel j} \rangle_{\mathbf{k}\omega} / n_j B_0) (B_0^2 / \langle \delta B_{\parallel j} \delta B_{\parallel j} \rangle_{\mathbf{k}\omega})$. However, it is evident from its definition that $C_{\parallel j}$ is related to C_j as well as to $R_{\parallel n_j}$. We use $R_{\parallel n_p}$ in order to have a quantity which is independent of C_j . We also add two transport ratios which involve only components of the fluctuating magnetic fields. The first of these we call the “magnetic compressibility”

$$C_B(\mathbf{k}, \omega) \equiv \frac{\langle \delta B_{\parallel} \delta B_{\parallel} \rangle_{\mathbf{k}\omega}}{\langle \delta \mathbf{B} \cdot \delta \mathbf{B} \rangle_{\mathbf{k}\omega}}, \quad (4)$$

and the second the “noncoplanar ratio”

$$R_{nc}(\mathbf{k}, \omega) \equiv \frac{\langle \delta B_x \delta B_x \rangle_{\mathbf{k}\omega}}{\langle \delta \mathbf{B} \cdot \delta \mathbf{B} \rangle_{\mathbf{k}\omega}}, \quad (5)$$

where, from the definition of our coordinate system, the y direction with the z direction defines the coplanarity plane of the fluctuation (the plane containing \mathbf{k} and \mathbf{B}_0). The magnetic compressibility C_B is functionally equivalent to the transverse ratio of *Song et al.* [1994]. The noncoplanar ratio R_{nc} gives additional information about the polarization of $\delta \mathbf{B}$. Although we include R_{nc} to gain theoretical insight, we will for the most part not make use of it in this paper because of the difficulty in establishing the direction of \mathbf{k} .

We estimate the transport ratios from finite time series of measured plasma moments and magnetic field. Low frequencies are neglected due to undersampling, and high frequencies ($f > 0.04$ Hz) are neglected to avoid certain difficulties due to uneven data sampling. Stationarity is checked by comparing spectra of shorter time series imbedded within the interval of interest.

Transport ratios are useful as identifiers of low-frequency fluctuations primarily because they can all be computed in the same way from observed field and plasma fluctuation spectra as well as from linear Vlasov theory. We have chosen these particular transport ratios because each one provides independent information and does not change its value under a change of reference frame.

The result that our identifiers are independent of reference frame is particularly important in the magnetosheath, where the plasma flows relative to the observing spacecraft are often of the order of the Alfvén and/or ion sound speeds. Such flows introduce significant Doppler shifts in the observed fluctuation frequencies, but do not change the values of the constituents of our transport ratios; that is, the fluctuating magnetic field components, the fluctuating ion density and the fluctuating ion velocity do not change under a Galilean velocity transformation as shown in Appendix A.

Transport Ratios: Theoretical Values

We have computed the transport ratios defined above through the use of a linear Vlasov dispersion code for $\beta_{\parallel p} = 0.10$, $\beta_{\parallel p} = 1.0$, and $\beta_{\parallel p} = 10.0$ using bi-Maxwellian zeroth-order distribution functions [*Gary*, 1992]. Other parameters are $T_e = T_{\parallel p}/4$, $(T_{\perp}/T_{\parallel})_p = 1 + 0.65\beta_{\parallel p}^{-0.40}$, and $kc/\omega_p = 0.10$, where k is the wave number, c is the speed of light, and $\omega_p \equiv \sqrt{4\pi n_p e^2/m_p}$ is the plasma frequency. The formula for $(T_{\perp}/T_{\parallel})_p$ is (3c) of *Gary et al.* [1994] and represents an inverse correlation between $(T_{\perp}/T_{\parallel})_p$ and $\beta_{\parallel p}$ appropriate for a proton/electron plasma such as is observed in the magnetosheath [*Anderson et al.*, 1994]. The range of real frequency ω/Ω_p and growth rate γ/Ω_p values normalized to the proton gyrofrequency Ω_p is shown for each mode in Table 2a. There is a range of values because of the range of θ_{kB} for each mode. We stress that the value of k is kept constant; thus the properties

of the waves are not calculated for maximum growth rate. Quasi-perpendicular and quasi-parallel modes are considered to be separate modes. The values of the transport ratios are given in Table 2b. The information in these tables is similar to that of Tables 2a and 2b of *Gary and Winske* [1992] but is more detailed. Under our present nomenclature, the ion acoustic mode at $\beta_{\parallel p} = 10$ corresponds to the Gary and Winske fast mode at $\theta_{kB} \lesssim 30^\circ$ and slow mode at $\theta_{kB} \gtrsim 60^\circ$. Similarly, our magnetosonic mode at $\beta_{\parallel p} = 10$ corresponds to Gary and Winske's slow mode at $\theta_{kB} \lesssim 30^\circ$, and their fast wave at $\theta_{kB} \gtrsim 60^\circ$. In Table 2, the notation “[a, b]” indicates that the range of values of a quantity is from a to b . The rough meanings of the other symbols are transparent, and the exact definitions are given at the bottom of the table.

From Table 2a, we see that at the relatively long wavelengths considered here, the only unstable mode is the quasi-perpendicular mirror mode at $\beta_{\parallel p} = 10.0$. If we somewhat arbitrarily define “lightly damped” as $\gamma/\Omega_p \geq -10^{-3}$, then the quasi-perpendicular mirror mode is lightly damped at $\beta_{\parallel p} = 1.0$ and 0.1. The Alfvén and magnetosonic modes are lightly damped for all circumstances with the exception of the quasi-perpendicular magnetosonic wave at $\beta_{\parallel p} = 10$. The ion acoustic mode is heavily damped at both quasi-

parallel and quasi-perpendicular propagation. (We have assumed $T_e \ll T_p$, which is characteristic of the magnetosheath.) This heavy damping had led *Gary and Winske* [1992] and *Gary* [1992] to dismiss the ion acoustic mode as a potential mode in the sheath. However, because there is evidence that this “slow” mode may be observed in the sheath, where it is perhaps driven by strong perturbations at the magnetopause [*Song et al.*, 1992], we will for completeness ignore this strong damping and permit the ion acoustic mode to compete in the identification process as though it were weakly damped. Similarly, the quasi-parallel mirror mode is heavily damped, but we will also let it compete as a potential mode.

Our procedure for mode identification consists of comparing the observed transport ratios for a particular fluctuation against those of Table 2; the mode which best matches the observations is identified as the mode in question. If an observed mode has values of C_B , R_{Ap} , C_p and $R_{\parallel n_p}$ within the theoretical ranges specified by Table 2, that mode can be, with one exception, uniquely identified using Table 2. (The magnetosonic and Alfvén modes cannot be distinguished at $0 < \theta_{kB} \lesssim 30^\circ$ without using R_{nc} .) We now demonstrate the uniqueness of identification using the $\beta_{\parallel p} = 0.1$ case as an example. The mirror mode, ion acoustic mode, and quasi-

Table 2a. Real Frequency ω/Ω_p and Growth Rate γ/Ω_p for $\beta_{\parallel p} = 0.10$, $\beta_{\parallel p} = 1.0$, and $\beta_{\parallel p} = 10.0$

$\beta_{\parallel p}$	Mode	θ_{kB} , deg	ω/Ω_p	γ/Ω_p
0.10	magnetosonic	[5,30]	0.11	$[-5 \times 10^{-5}, 0]$
		[60,85]	0.11	$[-2 \times 10^{-4}, -5 \times 10^{-5}]$
0.10	Alfvén	[5,30]	[0.089,0.099]	$\simeq 0$
		[65,85]	[0.009,0.044]	$\simeq 0$
0.10	ion acoustic	[5,30]	[0.030,0.036]	$[-4 \times 10^{-2}, -3 \times 10^{-2}]$
		[60,80]	[0.005,0.02]	$[-2 \times 10^{-2}, -6 \times 10^{-3}]$
0.10	mirror	[5,30]	0	$[-7 \times 10^{-2}, -2 \times 10^{-2}]$
		[60,85]	0	$[-8 \times 10^{-3}, -1 \times 10^{-3}]$
1.0	magnetosonic	[5,30]	[0.12,0.14]	$[-7 \times 10^{-3}, -3 \times 10^{-4}]$
		[60,85]	[0.16,0.17]	$[-3 \times 10^{-3}, -7 \times 10^{-4}]$
1.0	Alfvén	[5,30]	[0.099,0.11]	$[-7 \times 10^{-4}, -1 \times 10^{-4}]$
		[60,85]	[0.010,0.057]	$[-3 \times 10^{-5}, 0]$
1.0	ion acoustic	[5,30]	[0.087,0.11]	$[-1.1 \times 10^{-1}, -9 \times 10^{-2}]$
		[60,80]	[0.018,0.051]	$[-7 \times 10^{-2}, -2 \times 10^{-2}]$
1.0	mirror	[5,30]	0	$[-2 \times 10^{-1}, -5 \times 10^{-2}]$
		[60,85]	0	$[-5 \times 10^{-3}, -4 \times 10^{-5}]$
10.0	magnetosonic	[5,30]	[0.17,0.28]	$[-1 \times 10^{-1}, -1 \times 10^{-3}]$
		[60,85]	[0.36,0.39]	$[-1.3 \times 10^{-2}, -5 \times 10^{-3}]$
10.0	Alfvén	[5,30]	[0.13,0.14]	$[-7 \times 10^{-3}, -2 \times 10^{-4}]$
		[60,85]	[0.013,0.076]	$[-1.5 \times 10^{-3}, -4 \times 10^{-4}]$
10.0	ion acoustic	[5,30]	[0.26,0.36]	$[-4 \times 10^{-1}, -3 \times 10^{-1}]$
		[60,80]	[0.055,0.158]	$[-2 \times 10^{-1}, -6 \times 10^{-2}]$
10.0	mirror	[5,30]	0	$[-7 \times 10^{-1}, -5 \times 10^{-2}]$
		[60,85]	0	$[+2 \times 10^{-3}, +9 \times 10^{-3}]$

Key to symbols in this table: $\simeq 0$ corresponds to (\Leftrightarrow) x such that $0 \leq x \leq 10^{-5}$ (which is zero to the accuracy of the calculation); $[a, b] \Leftrightarrow a \leq x \leq b$. Other parameters are $T_e = T_{\parallel p}/4$, $(T_{\perp}/T_{\parallel})_p = 1 + 0.65\beta_{\parallel p}^{-0.40}$, and $k_c/\omega_p = 0.10$.

Table 2b. Transport Ratios for $\beta_{\parallel p} = 0.10$, $\beta_{\parallel p} = 1.0$, and $\beta_{\parallel p} = 10.0$

$\beta_{\parallel p}$	Mode	θ_{kB} , deg	C_B	R_{nc}	R_{Ap}	C_p	$R_{\parallel n_p}$
0.10	magnetosonic	[5,30]	[0, 0.25]	[0, 0.5]	[0.9, 1.1]	[0, 0.3]	= 1
		[60,85]	[0.75, 1.0]	$\simeq 0$	[1.2, 1.3]	[0.8, 1.0]	= 1
0.10	Alfvén	[5,30]	$\simeq 0$	[0.5, 1.0]	[1.1, 1.2]	$\simeq 0$	= 1
		[65,85]	$\simeq 0$	= 1	$\simeq 1$	$\simeq 0$	$\simeq -1$
0.10	ion acoustic	[5,30]	[0, 0.25]	$\simeq 0$	≥ 130.0	≥ 500.0	$\simeq -1$
		[60,80]	[0.75, 1.0]	$\simeq 0$	≥ 160.0	≥ 620.0	$\simeq -1$
0.10	mirror	[5,30]	[0, 0.25]	$\simeq 0$	[1.0, 2.7]	[1.0, 15.0]	$= -1$
		[60,85]	[0.75, 1.0]	$\simeq 0$	[0.2, 0.5]	[8.0, 11.0]	$= -1$
1.0	magnetosonic	[5,30]	[0, 0.25]	[0, 0.5]	[1.2, 2.3]	[0, 0.7]	[0.76, 1.0]
		[60,85]	[0.75, 1.0]	$\simeq 0$	[2.6, 2.9]	$\simeq 1$	= 1
1.0	Alfvén	[5,30]	$\simeq 0$	[0.5, 1.0]	[1.3, 1.5]	$\simeq 0$	[0.7, 0.8]
		[60,85]	$\simeq 0$	$\simeq 1$	[1.3, 1.4]	$\simeq 0$	$\simeq -1$
1.0	ion acoustic	[5,30]	[0, 0.25]	$\simeq 0$	≥ 200.0	[70.0, 1000.0]	[-1.0, -0.4]
		[60,80]	[0.75, 1.0]	$\simeq 0$	≥ 510.0	≥ 170.0	$\simeq -1$
1.0	mirror	[5,30]	[0, 0.25]	$\simeq 0$	[1.3, 8.4]	[0.4, 3.0]	$= -1$
		[60,85]	[0.75, 1.0]	$\simeq 0$	$\simeq 0$	[0.2, 0.4]	$= -1$
10.0	magnetosonic	[5,30]	[0, 0.23]	[0, 0.5]	[2.8, 17.0]	[0, 1.1]	[-0.1, 0.6]
		[60,85]	[0.74, 1.0]	$\simeq 0$	[14.0, 16.0]	$\simeq 1$	= 1
10.0	Alfvén	[5,30]	$\simeq 0$	[0.5, 1.0]	[2.0, 2.3]	$\simeq 0$	[0, 0.2]
		[60,85]	$\simeq 0$	$\simeq 1$	= 2.3	$\simeq 0$	[-0.5, -0.4]
10.0	ion acoustic	[5,30]	[0, 0.23]	[0, 0.4]	≥ 800.0	[30.0, 1200.0]	[-0.9, -0.1]
		[60,80]	[0.7, 1.0]	$\simeq 0$	≥ 2900.0	[90.0, 130.0]	$\simeq -1$
10.0	mirror	[5,30]	[0, 0.25]	[0, 0.3]	[0, 70.0]	[0, 1.7]	$= -1$
		[60,85]	[0.75, 1.0]	$\simeq 0$	$\simeq 0$	$\simeq 0$	$= -1$

Key to symbols in this table: $\simeq 0$ corresponds to (\Leftrightarrow) x such that $0 \leq x \leq 0.10$; $\simeq 1 \Leftrightarrow 0.90 \leq x \leq 1.1$; $= 1 \Leftrightarrow 0.99 \leq x \leq 1.01$; $\geq a \Leftrightarrow x \geq a$; $[a, b] \Leftrightarrow a \leq x \leq b$. Other parameters are $T_e = T_{\parallel p}/4$, $(T_{\perp}/T_{\parallel})_p = 1 + 0.65\beta_{\parallel p}^{-0.40}$, and $kc/\omega_p = 0.10$.

perpendicular ($Q-\perp$) Alfvén wave have density and magnetic fluctuations out of phase, and thus $R_{\parallel n_p} < 0$. The Alfvén wave, with its fluctuations perpendicular to \mathbf{k} , has a small density perturbation and is distinguished from the other two modes by a small value of C_p . At $\theta_{kB} = 0$, the ion acoustic mode is purely electrostatic for which $\delta\mathbf{B} = 0$. The ion acoustic mode maintains a predominantly electrostatic character at other values of θ_{kB} , and Table 2 shows that it can be distinguished by large values of R_{Ap} and C_p . Magnetic fluctuations dominate for the mirror mode which can be distinguished by small values of R_{Ap} and C_p . (Note that McKean *et al.* [1992] in fact have found the small value of R_{Ap} for the mirror instability useful for distinguishing this mode from the Alfvén-like ion cyclotron instability in their simulations.) The value of C_B determines whether the mirror mode or ion acoustic mode are quasi-parallel ($Q-\parallel$) or quasi-perpendicular.

The three modes with plasma and magnetic field fluctuating together in phase ($R_{\parallel n_p} \simeq 1$) are the $Q-\parallel$ and $Q-\perp$ magnetosonic mode and the $Q-\parallel$ Alfvén mode. For the quasi-perpendicular magnetosonic mode, C_B and C_p are near unity due to the compressional nature of the mode. The value of R_{nc} would be useful to distinguish the $Q-\parallel$ magnetosonic and Alfvén modes. The Alfvén mode has fluctuations predominantly out of the coplanarity plane (the plane containing both \mathbf{k} and \mathbf{B}_0), whereas the other modes have fluctuations pre-

dominantly in the coplanarity plane; thus R_{nc} should be small for all modes except the Alfvén mode. However, at low $\beta_{\parallel p}$ and low frequency, the $Q-\parallel$ Alfvén and magnetosonic modes are essentially the same mode, differing only in the direction of the fluctuating magnetic field in the plane perpendicular to \mathbf{B}_0 .

Two of our transport ratios, R_{Ap} and C_p , are defined as the ratio of two totally independent quantities and have values which can vary between zero and infinity. We map the possibly infinite variation of these quantities to a total range of two according to the following ratio mapping \mathcal{M} of the quantity q

$$\begin{aligned}\mathcal{M}(q) &= q, & \text{for } q \leq 1 \\ \mathcal{M}(q) &= 2 - \frac{1}{q}, & \text{for } q > 1.\end{aligned}\quad (6)$$

We use $\mathcal{M}(R_{Ap})$ and $\mathcal{M}(C_p)$ rather than R_{Ap} and C_p to get a measure of the difference of observed and theoretical values for these transport ratios. The ratio mapping \mathcal{M} has the property that $|\mathcal{M}(q_1) - \mathcal{M}(q_2)| = |\mathcal{M}(1/q_1) - \mathcal{M}(1/q_2)|$ which is desirable because we could just as well have defined R_{Ap} or C_p as the inverse of their definitions.

Figures 1a-1d display the information of Table 2 pictorially. For each mode there is a range of values for C_B , $\mathcal{M}(R_{Ap})$, $\mathcal{M}(C_p)$, and $R_{\parallel n_p}$ for three different values of $\beta_{\parallel p}$. We take the midpoint of each range of a transport ratio to get a point in C_B - $\mathcal{M}(R_{Ap})$ - $\mathcal{M}(C_p)$ - $R_{\parallel n_p}$

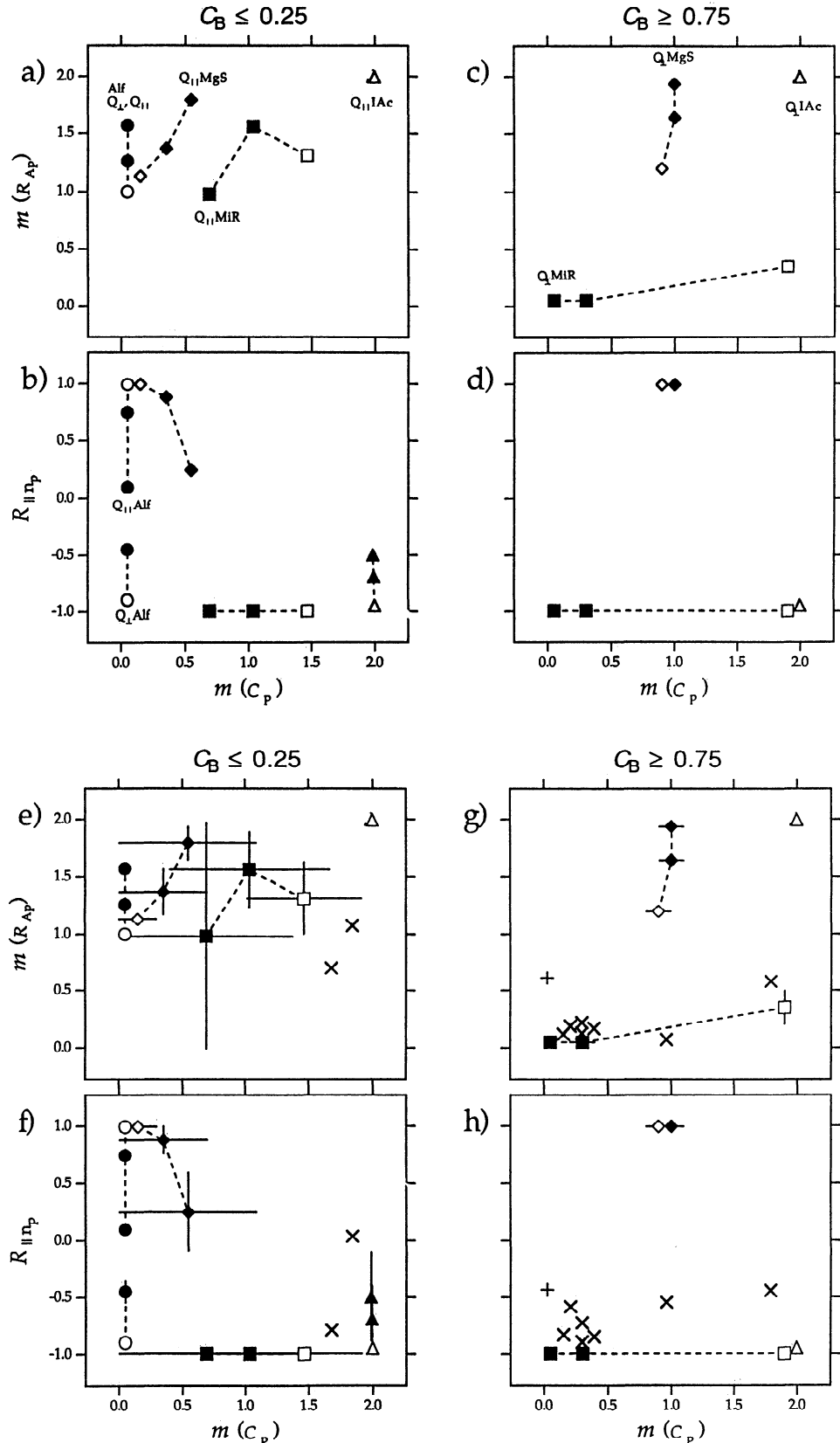


Figure 1. (a) $\mathcal{M}(R_{Ap})$ and (b) $R_{\parallel n_p}$ versus $\mathcal{M}(C_p)$ for $C_B \leq 0.25$. The theoretical values for each mode are plotted for $\beta_{\parallel p} = 0.10$, $\beta_{\parallel p} = 1.0$, and $\beta_{\parallel p} = 10.0$ with the open symbol indicating the low $\beta_{\parallel p} = 0.10$ value. (c and d) Same as Figures 1a and 1b except for $C_B \geq 0.75$. (e-h) Same as Figures 1a-1d except the observed events have been added, with the plus (cross) indicating an event with $\beta_{\parallel p} > 1$ ($\beta_{\parallel p} < 1$). Also the theoretical mode values now have error bars.

space for each value of $\beta_{\parallel p}$ and for each mode. Figures 1a and 1b display points for the five modes with $C_B \leq 0.25$, the $Q-\parallel$ and $Q-\perp$ Alfvén and the $Q-\parallel$ magnetosonic, ion acoustic and mirror modes, whereas Figures 1c and 1d display points for the three modes with $C_B \geq 0.75$, the $Q-\perp$ magnetosonic, ion acoustic and mirror modes. The values of $\mathcal{M}(R_{Ap})$ are plotted versus $\mathcal{M}(C_p)$ in Figures 1a and 1c while values of $R_{\parallel n_p}$ versus $\mathcal{M}(C_p)$ are plotted in Figures 1b and 1d. For each mode, three symbols connected by a dashed line indicate the values of the transport ratios at $\beta_{\parallel p} = 0.10$, $\beta_{\parallel p} = 1.0$, and $\beta_{\parallel p} = 10.0$. The open symbol is for the low $\beta_{\parallel p} = 0.10$. A single open symbol is plotted if the values of transport ratios overlap at all values of $\beta_{\parallel p}$. The abbreviation “MgS” and the diamond symbol are used for the magnetosonic mode, “Alf” and the circle symbol for the Alfvén mode, “IAc” and the triangle symbol for the ion acoustic mode, and “Mir” and the square symbol for the mirror mode.

Definition of the Mode Deviation $D(\text{mode})$

Because the observed transport ratios may not be in total agreement with any mode, it is not immediately obvious how the various transport ratios should be used in concert to determine the most probable mode. In the magnetosheath plasma there are complicating factors like inhomogeneities, nonlinear effects, random noise, and the possible presence of more than one mode. It is desirable therefore to have some means to assess whether the collection of transport ratios provides a good identification of the wave.

One could arrange the transport ratios in a logical hierarchy whereby one compares the observed values against the theoretical predictions first for one ratio and then for others in a specified decision sequence [Song *et al.*, 1994]. This technique gives the greatest weight to the first ratio used in the logical decision sequence and little weight to ratios used only late in the scheme. Hence it does not make full use of the information available in the set of independent transport ratios. Furthermore, the identification of the mode may depend on which ratio is used first. It seems more appropriate to combine all of the transport ratios simultaneously to yield a single measure of the separation of the observed fluctuation properties and theoretical predictions for each mode.

To do this, we begin by mapping the values of R_{Ap} and C_p to a variation range of two using the ratio mapping $\mathcal{M}()$ described by (6). We multiply the values of C_B by 2, so it also varies over the range 0 to 2. The value of $R_{\parallel n_p}$ already has a variation range of two, from -1 to +1. For a given mode m and transport ratio t , we define the deviation D_{mt} as the absolute value of the difference between the observed transport ratio and the mode theoretical value. In general, the mode theoretical values may be represented by a range of values (as in Table 2) and the observed values may also be

represented by a range of values due to the error. In such a case we let D_{mt} be zero if the ranges overlap. If the ranges do not overlap, D_{mt} is equal to the smallest difference between any value in the theoretical range and any value in the observational range. Finally, for each mode, we define the total deviation $D(m)$ as the root mean square value of the transport ratio deviations D_{mt} , that is,

$$D(m) = \left(\frac{1}{N_T} \sum_t D_{mt}^2 \right)^{1/2}, \quad (7)$$

where m represents one of the eight modes of Table 2 and N_T is the number of transport ratios used (in our case, four).

If the mode deviation $D(m)$ is zero, then the mode theoretical transport ratios are in total agreement with the observed ratios. If the mode deviation is two, the observed mode has exactly the opposite properties of the theoretical mode (if the observed R_{Ap} is 0, the mode R_{Ap} must be infinity; and if the observed $R_{\parallel n_p}$ is -1, the theoretical value must be +1). A mode deviation of order unity represents no agreement between the observed and theoretical values. Thus we consider the observed mode to be in good agreement with the theoretical mode if $D(m) \ll 1$.

If more than one theoretical mode has a small value of $D(m)$, then both theoretical modes agree with the observations. In general, we consider the observed mode to be well identified as the best fitting mode if the smallest value of $D(m)$ is less than the difference between the next smallest $D(m)$ and the smallest $D(m)$. (If both modes have very small $D(m)$, say less than 0.1, we would consider them both to be essentially in total agreement with the observations: therefore the mode would not be well identified. However, in this paper there was no case where the smallest $D(m)$ was less than the difference to the next smallest $D(m)$ and both were less than 0.1.)

Note that in order for $D(m)$ to indicate the net mode deviation, it was necessary that all the transport ratios be independent (which led to the use of $R_{\parallel n_p}$) and that they vary over the same range (which led to the use of (6)).

IRM Data

The ion density and velocity are measured by the IRM spacecraft every spin period, which is approximately 4.3 s [Paschmann *et al.*, 1985]. Since IRM has no ion composition information, we assume the ion fluctuations to be predominantly due to proton fluctuations (see Paschmann *et al.* [1986] for a discussion of the error involved). From the plasma data we can calculate the Fourier transforms necessary to calculate the transport ratios. We do linear detuning (subtract the linear fit to get fluctuating quantities) and apply a Welsh window before Fourier transforming. The highest possible frequency for calculating transport ratios based on the

plasma fluctuations is the Nyquist frequency, which is approximately 0.1 Hz.

The magnetic field data are sampled at a much higher rate, every 31 or 62 ms depending on the mode of operation [Lühr *et al.*, 1985]. Spin averages of the magnetic field data were used in computing the transport coefficients, since these matched the time resolution of the plasma data. However, the full-resolution magnetic field data were used as a check. We have confined our study to frequencies below 0.04 Hz, and for these frequencies the low-resolution data are in qualitative agreement with the high-resolution data for all cases.

Example Case

We first consider the same time segment as was recently analyzed by Song *et al.* [1994], September 1, 1984, 0642–0718 UT. This time segment starts about 3 min after an outbound magnetopause crossing, and the average plasma density and magnetic field were roughly constant over the interval. Figure 2 displays, from top to bottom, the low-frequency power spectra $|\delta B|^2/\Delta f$ (nT^2/Hz) of magnetic fluctuations parallel (solid) and perpendicular (dashed) to \mathbf{B}_0 , C_B , R_{Ap} , C_p , and $R_{\parallel n_p}$, as a function of frequency in hertz. These quantities are found from the Fourier-transformed magnetic and plasma data using the definitions in (1)–(4). The frequencies here are all well below the proton gyrofrequency F_{cp} ($= \Omega_p/(2\pi)$), which is 0.604 Hz. The power spectra of the magnetic field fluctuations found from the high-resolution magnetic data (not shown) agree well with those found from the low-resolution data except at frequencies $\gtrsim 0.06$ Hz.

From 0 to 0.06 Hz there appear to be two distinct regions of waves, one with predominantly perpendicular fluctuations from 0 to 0.01 Hz, and the second with predominantly parallel fluctuations from 0.01 to 0.06 Hz. We will not try to identify the lower-frequency waves since they peak at zero frequency and are therefore not well represented using a finite time Fourier transform. Limiting ourselves to the range 0.01–0.04 Hz we find $C_B \lesssim 1$, $R_{Ap} < 0.3$, $C_p < 0.25$, and $R_{\parallel n_p} \simeq -1$. For this event, $\beta_{\parallel p} = 0.86$. From Table 2, we see then that the observed transport ratios are in general agreement with the values for the $Q-\perp$ mirror mode, but not with those of any other mode.

Now we consider more carefully the peak in parallel power at a frequency of 0.027 Hz. Values of C_B , R_{Ap} , C_p , and $R_{\parallel n_p}$ at this peak are given in Table 3 in the row marked “Observed.” Because the value of C_B is so large (0.91), the mode responsible for this peak must be either the quasi-perpendicular magnetosonic, ion acoustic, or mirror mode (see Table 2 or Figure 1). In order to verify our mode identification based on the rough values of transport ratios from Table 2, we have calculated the theoretical transport ratios for all four quasi-perpendicular modes, including the Alfvén mode, using the measured ion density, temperature, and magnetic field strength averaged over the interval. These are listed in Table 3. We calculated the transport ra-

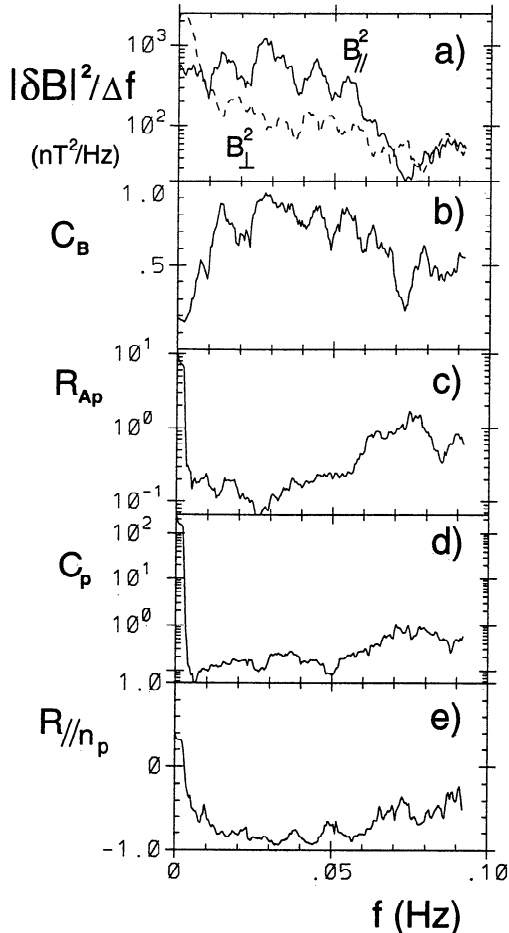


Figure 2. (a) Power spectra $|\delta B|^2/\Delta f$ (nT^2/Hz) of magnetic fluctuations parallel (solid) and perpendicular (dashed) to \mathbf{B}_0 , (b) C_B , (c) R_{Ap} , (d) C_p , and (e) $R_{\parallel n_p}$ versus frequency in hertz for the September 1, 1984, event (event 9 in Table 4a). $F_{cp} = 0.60$ Hz.

tios over a range of angles θ_{kB} and wave numbers k . The details of our plasma model and the values of θ_{kB} and k we used are explained in Appendix B. In Table 3 the first number given for a theoretical transport ratio is the value at the middle values of θ_{kB} and k . The minimum and maximum theoretical values over the entire range of θ_{kB} and k considered are given by the two following numbers in brackets. From the values in Table 3 it is clear that the observed transport ratios are closer to the mirror mode values than to those of any of the other modes. The observed R_{Ap} lies within the theoretical range of mirror mode values. Although the observed values of C_p and $R_{\parallel n_p}$ do not lie within the range of mirror values given in the table, they lie quite close (within a 50% variation of one of the range limits). None of the other theoretical modes comes close to describing the observed transport ratios. In the last column of Table 3 the mode deviation is listed for each theoretical mode. The mirror mode has a small deviation, $D(Q-\perp \text{ Mir}) = 0.09 \ll 1$, while each of the other modes has $D(\text{mode}) \geq 1$. Thus we consider the wave mode in this case to be well identified. The agree-

Table 3. Comparison of Observed Transport Ratios to Quasi-Perpendicular ($60^\circ \leq \theta_{kB} \leq 80^\circ$) Mode Values for September 1, 1984, Case

Mode	C_B	R_{Ap}	C_p	$R_{\parallel n_p}$	$D(\text{Mode})$
Observed	0.91	0.075	0.12	-0.87	...
Magnetosonic	0.88 [0.75,0.97]	2.33 [2.28,2.42]	0.96 [0.93,0.99]	1.000 [1.000,1.000]	1.26
Alfvén	0.002 [0.00015,0.044]	1.16 [1.05,1.17]	0.003 [0.00059,0.041]	-0.96 [-0.98,-0.94]	1.00
Ion acoustic	0.88 [0.75,0.97]	520. [450.,550.]	194. [171.,202.]	-0.995 [-0.996,-0.993]	1.34
Mirror	0.88 [0.75,0.97]	0.038 [0.013,0.12]	0.30 [0.25,0.40]	-1.000 [-1.000,-1.000]	0.09

ment with the ion acoustic mode is exceptionally poor with $D(Q-\perp \text{IAc}) = 1.34$. Thus we disagree with *Song et al.* [1994], who identified these waves as the “slow mode” (our ion acoustic mode). (Note, however, that our result was anticipated by Appendix B of *Song et al.* [1994].) The best identification of the waves is the mirror mode.

Survey of Waves In the Magnetosheath Close to the Magnetopause

We have examined the IRM data for 20 magnetopause crossings in order to determine what low-frequency modes are observed in the magnetosheath close to the magnetopause. We chose data segments for the more detailed analysis to follow based on the following limited set of information: time series plots of ion density and the three components of magnetic field, and parallel and perpendicular magnetic power spectra computed over 5 min time intervals. The plots of power spectra also indicated the sign of $R_{\parallel n_p}$. (This limited set of quantities was chosen because from them it is impossible to differentiate the $Q-\perp$ mirror mode from the $Q-\perp$ ion acoustic mode. One of the goals of this study was to determine which of these two modes was more important for the production of parallel magnetic fluctuations observed in the vicinity of the magnetopause. Our method of data selection ensured that we did not preselect the data in favor of either one of these modes.) We picked out time intervals of 5 to 38 min duration during which the ion density, magnetic field, power spectra, and sign of $R_{\parallel n_p}$, were roughly constant. No event was temporally more than 21 min from a magnetopause crossing, and most were much closer. We eliminated three of the crossings because of data gaps; we allowed no gap longer than 14 s. (We tried to identify the wave mode for these cases despite the presence of data gaps; none of these had well-identified waves.) Thus we have events corresponding to 17 magnetopause crossings.

Table 4a gives an event number, date, start and stop time, duration, time from magnetopause crossing, frequency range used in this study, the proton gyrofrequency F_{cp} , and frequency range normalized to the proton gyrofrequency F/F_{cp} . In the last section we used the transport ratios at the frequency for which the parallel magnetic fluctuations were a peak. For the remaining analysis we evaluate the transport ratios over a range of frequency (given for each event in Table 4a).

We use the average value over the frequency range for C_B and $R_{\parallel n_p}$, and the log average value for R_{Ap} and C_p , weighting the values at each frequency by the total magnetic power at that frequency.

We avoided frequencies below 0.01 Hz because of the small number of wave periods sampled at such a low frequency. We have also limited the maximum frequency to 0.04 Hz in order to avoid complications in the Fourier analysis at higher frequencies due to the fact that in the most common mode, the plasma data were not sampled evenly [Paschmann *et al.*, 1985]. In all but one case the dominant waves were below 0.04 Hz. (In that one case, November 3, 1985, event 11, there were two significant peaks in power, one at frequency above and one at frequency below 0.045 Hz.) Except for this one case, a single frequency range appeared adequate to characterize the waves for each event (at least excluding frequencies lower than 0.01 Hz). The most common frequency range we used is 0.01–0.04 Hz. For all but the last three events (at highest $\beta_{\parallel p}$), $F/F_{cp} < 0.1$; for the last three events, $F/F_{cp} < 0.2$.

The value of $\beta_{\parallel p}$, proton temperature ratio $(T_\perp/T_\parallel)_p$, ratio of wave to background magnetic energy $|\delta\mathbf{B}|^2/B_0^2$, and values of the transport ratios C_B , R_{Ap} , C_p , and $R_{\parallel n_p}$, are listed for each event in Table 4b. As can be seen from the values of $\beta_{\parallel p}$, we have ordered the events by $\beta_{\parallel p}$ rather than by the date. The errors for R_{Ap} and C_p are multiplicative, as they are found from the standard deviation of the log value.

In Figure 3 we plot the values of C_B , R_{Ap} , C_p , and $R_{\parallel n_p}$ for the 17 events of Table 4b versus $\beta_{\parallel p}$. Events with $C_B \geq 0.75$ (parallel magnetic fluctuations dominant) are plotted as pluses and events with $C_B \leq 0.25$ (perpendicular magnetic fluctuations dominant) are plotted as crosses; the intermediate values are plotted as circles. The crosses (representing low values of C_B , or $\delta B_\parallel \ll \delta B$) occur at low values of $\beta_{\parallel p}$, perhaps because the plasma will tend to be incompressible at low $\beta_{\parallel p}$. At very high values of $\beta_{\parallel p}$, the background magnetic field direction becomes irrelevant and we find $C_B \sim 0.5$. In the other panels we do not notice any significant difference between the points with pluses, crosses, or circles. The only clear trend with $\beta_{\parallel p}$ is in C_p . There is a striking variation in C_p from very large values at low $\beta_{\parallel p}$ to very small values at high $\beta_{\parallel p}$. This dramatic dependence of C_p with $\beta_{\parallel p}$ shows that the data as a whole are consistent with, and only consistent with, the mirror mode, as can be seen from Table 2 or Figure 1.

Table 4a. Event Data: General Information

Event	Date	UT Start	UT End	Duration, min	Minutes from Magnetopause	Frequency, Hz	F_{cp} , Hz	F/F_{cp}
1	Oct. 6, 1984	0709:10	0713:41	5	15	[0.01, 0.04]	1.4	[0.0071, 0.029]
2	Oct. 24, 1985	1255:00	1301:20	6	2	[0.01, 0.04]	0.96	[0.010, 0.042]
3	Oct. 8, 1985	0900:00	0911:06	11	3	[0.01, 0.04]	0.88	[0.011, 0.045]
4	Nov. 12, 1984	0651:38	0657:46	6	10	[0.01, 0.03]	0.64	[0.016, 0.047]
5	Sept. 21, 1984	1313:19	1335:49	23	3	[0.01, 0.04]	0.73	[0.014, 0.055]
6	Oct. 24, 1985	1228:20	1243:00	15	21	[0.01, 0.04]	0.66	[0.015, 0.061]
7	Nov. 17, 1985	1232:41	1243:07	10	20	[0.01, 0.04]	0.79	[0.013, 0.051]
8	Oct. 9, 1984	1147:40	1353:20	6	13	[0.02, 0.04]	0.62	[0.032, 0.065]
9	Sept. 1, 1984	0642:00	0719:58	38	3	[0.01, 0.04]	0.60	[0.017, 0.067]
10	Sept. 25, 1984	0610:00	0622:28	11	3	[0.015, 0.04]	0.51	[0.029, 0.078]
11	Nov. 3, 1985	0548:21	0558:24	10	9	[0.01, 0.04]	0.48	[0.021, 0.083]
12	Sept. 14, 1984	0448:25	0501:07	13	3	[0.01, 0.04]	0.50	[0.020, 0.080]
13	Sept. 28, 1984	1148:20	1200:03	12	15	[0.02, 0.04]	0.41	[0.049, 0.098]
14	Oct. 24, 1984	0912:01	0918:52	7	21	[0.01, 0.04]	0.54	[0.019, 0.074]
15	Oct. 8, 1985	0945:49	0956:01	10	5	[0.025, 0.05]	0.29	[0.086, 0.17]
16	Nov. 3, 1985	0516:41	0526:45	10	11	[0.01, 0.04]	0.28	[0.036, 0.14]
17	Sept. 17, 1984	2200:06	2210:55	11	14	[0.023, 0.04]	0.21	[0.11, 0.19]

Table 4b. Event Data: Transport Ratios

Event	$\beta_{\parallel p}$	$\left(\frac{T_{\perp}}{T_{\parallel}}\right)_p$	$\frac{ B^2 }{B_0^2}$	C_B	R_{Ap}	C_p	$R_{\parallel n_p}$
1	0.033	4.60	0.00062	0.03 ± 0.05	$1.1 \times / 2.3$	$6.1 \times / 2.4$	0.04 ± 0.31
2	0.086	2.98	0.00077	0.78 ± 0.05	$0.58 \times / 1.7$	$4.8 \times / 2.1$	-0.44 ± 0.30
3	0.2	1.11	0.0020	0.14 ± 0.06	$0.70 \times / 1.4$	$3.1 \times / 1.5$	-0.79 ± 0.11
4	0.44	1.75	0.0032	0.84 ± 0.13	$0.072 \times / 1.6$	$0.96 \times / 1.6$	-0.55 ± 0.27
5	0.54	1.86	0.018	0.91 ± 0.04	$0.19 \times / 1.6$	$0.21 \times / 1.8$	-0.59 ± 0.23
6	0.54	1.89	0.016	0.91 ± 0.05	$0.13 \times / 1.6$	$0.30 \times / 1.4$	-0.90 ± 0.08
7	0.63	1.87	0.011	0.88 ± 0.05	$0.17 \times / 1.8$	$0.39 \times / 1.4$	-0.85 ± 0.09
8	0.72	1.90	0.013	0.81 ± 0.08	$0.22 \times / 1.6$	$0.30 \times / 1.3$	-0.73 ± 0.13
9	0.86	1.50	0.015	0.81 ± 0.09	$0.12 \times / 1.4$	$0.15 \times / 1.3$	-0.84 ± 0.07
10	1.3	1.28	0.050	0.48 ± 0.18	$0.24 \times / 1.9$	$0.071 \times / 1.8$	-0.64 ± 0.18
11	1.3	1.63	0.0090	0.66 ± 0.12	$1.8 \times / 1.5$	$0.15 \times / 1.6$	-0.66 ± 0.21
12	1.47	1.45	0.041	0.36 ± 0.14	$0.28 \times / 1.6$	$0.091 \times / 2.7$	-0.45 ± 0.39
13	2.1	1.36	0.013	0.79 ± 0.12	$0.61 \times / 2.6$	$0.025 \times / 2.4$	-0.44 ± 0.25
14	2.1	1.45	0.037	0.67 ± 0.13	$0.19 \times / 1.7$	$0.097 \times / 1.6$	-0.73 ± 0.13
15	3.2	1.43	0.012	0.54 ± 0.20	$0.79 \times / 1.2$	$0.061 \times / 2.1$	-0.15 ± 0.46
16	8.9	1.01	0.17	0.44 ± 0.19	$0.47 \times / 1.9$	$0.033 \times / 1.7$	-0.30 ± 0.37
17	9.4	0.95	0.10	0.31 ± 0.07	$0.18 \times / 1.3$	$0.007 \times / 2.5$	-0.12 ± 0.45

The notation “ $\times /$ ” indicates a multiplicative error factor determined from the standard deviation of the log value.

We plotted the values of the theoretical mode transport ratios for $C_B \leq 0.25$ in Figures 1a and 1b and for $C_B \geq 0.75$ in Figures 1c and 1d. The format of Figures 1e–1h is the same as that of Figures 1a–1d except that the event data values have been plotted as well. Events with $C_B \leq 0.25$ are plotted in Figures 1e and 1f and events with $C_B \geq 0.75$ are plotted in Figures 1g and 1h. In Figures 1e–1h, events with $\beta_{\parallel p} > 1$ have been plotted as pluses while events with $\beta_{\parallel p} < 1$ have been plotted as crosses. Error bars have also been added for the mode theoretical values. From the plot for $C_B \geq 0.75$, it is immediately evident that a large number of events cluster around mirror mode

theoretical values. The best identification for the two events with $C_B \leq 0.25$ is not quite as clear, but it appears that the points are closer to the mirror values than to any other mode.

We have calculated the mode deviations for each of the eight modes and listed these in Table 4c. Based on the practical equivalence between the theoretical values from Table 2 and values found using the measured plasma parameters for the September 1, 1984, case examined in the last section, we used Table 2 values for the mode theoretical range of transport ratio values to calculate the mode deviations. Table 4d summarizes the information in Table 4c and represents theulti-

Table 4c. Event Data: Mode Deviations

Event	Deviations							
	$Q-\parallel$ MgS	$Q-\perp$ MgS	$Q-\parallel$ Alf	$Q-\perp$ Alf	$Q-\parallel$ IAc	$Q-\perp$ IAc	$Q-\parallel$ Mir	$Q-\perp$ Mir
1	0.73	0.80	0.82	0.82	0.37	0.77	0.36	0.76
2	0.98	0.64	1.12	0.97	0.71	0.53	0.49	0.12
3	0.97	1.04	1.06	0.70	0.51	0.75	0.06	0.55
4	0.89	0.92	1.01	0.83	1.10	1.00	0.70	0.09
5	0.95	0.94	1.05	0.88	1.32	1.18	0.77	0.16
6	1.12	1.13	1.21	0.90	1.34	1.19	0.78	0.12
7	1.06	1.08	1.15	0.85	1.25	1.11	0.73	0.02
8	0.94	1.03	1.02	0.76	1.24	1.15	0.65	0.07
9	1.03	1.18	1.10	0.81	1.36	1.28	0.71	0.07
10	0.68	1.02	0.70	0.45	1.21	1.21	0.35	0.13
11	0.63	0.79	0.69	0.44	0.93	0.89	0.30	0.53
12	0.52	0.90	0.54	0.44	1.16	1.19	0.30	0.26
13	0.54	0.74	0.66	0.57	1.10	1.02	0.46	0.17
14	0.80	1.13	0.85	0.68	1.28	1.25	0.40	0.07
15	0.25	0.66	0.31	0.33	1.07	1.08	0.21	0.34
16	0.36	0.81	0.31	0.35	1.10	1.12	0.16	0.21
17	0.69	1.07	0.63	0.67	1.31	1.37	0.21	0.43

Key to modes: $Q-\parallel$ corresponds to (\Leftrightarrow) $5^\circ < \theta_{kB} \lesssim 30^\circ$; $Q-\perp$ (\Leftrightarrow) $60^\circ \lesssim \theta_{kB} < 85^\circ$; MgS (\Leftrightarrow) Magnetosonic; Alf (\Leftrightarrow) Alfvén; IAc (\Leftrightarrow) Ion Acoustic; Mir (\Leftrightarrow) Mirror.

Table 4d. Event Data: Best Fitting Modes

Event	C_B	Best Fitting Mode	$D(\text{Best})$	$D(\text{Second}) - D(\text{Best})$	Second Best Mode	$D(\text{Third}) - D(\text{Best})$	Third Best Mode	Well Identified
1	0.03	$Q-\parallel$ Mir	0.36	0.01	$Q-\parallel$ IAc			
2	0.78	$Q-\perp$ Mir	0.12	0.37	$Q-\parallel$ Mir	0.40	$Q-\perp$ IAc	$Q-\perp$ Mir
3	0.14	$Q-\parallel$ Mir	0.06	0.45	$Q-\parallel$ IAc			$Q-\parallel$ Mir
4	0.84	$Q-\perp$ Mir	0.09	0.61	$Q-\parallel$ Mir	0.74	$Q-\perp$ Alf	$Q-\perp$ Mir
5	0.91	$Q-\perp$ Mir	0.16	0.60	$Q-\parallel$ Mir	0.71	$Q-\perp$ Alf	$Q-\perp$ Mir
6	0.91	$Q-\perp$ Mir	0.12	0.66	$Q-\parallel$ Mir	0.78	$Q-\perp$ Alf	$Q-\perp$ Mir
7	0.88	$Q-\perp$ Mir	0.02	0.70	$Q-\parallel$ Mir	0.83	$Q-\perp$ Alf	$Q-\perp$ Mir
8	0.81	$Q-\perp$ Mir	0.07	0.58	$Q-\parallel$ Mir	0.69	$Q-\perp$ Alf	$Q-\perp$ Mir
9	0.81	$Q-\perp$ Mir	0.07	0.64	$Q-\parallel$ Mir	0.74	$Q-\perp$ Alf	$Q-\perp$ Mir
10	0.48	$Q-\perp$ Mir	0.13	0.22	$Q-\parallel$ Mir	0.33	$Q-\perp$ Alf	$Q-\perp$ Mir
11	0.66	$Q-\parallel$ Mir	0.30	0.14	$Q-\perp$ Alf			
12	0.36	$Q-\perp$ Mir	0.26	0.04	$Q-\parallel$ Mir	0.18	$Q-\perp$ Alf	
13	0.79	$Q-\perp$ Mir	0.17	0.28	$Q-\parallel$ Mir	0.37	$Q-\parallel$ MgS	$Q-\perp$ Mir
14	0.67	$Q-\perp$ Mir	0.07	0.33	$Q-\parallel$ Mir	0.61	$Q-\perp$ Alf	$Q-\perp$ Mir
15	0.54	$Q-\parallel$ Mir	0.21	0.03	$Q-\parallel$ MgS			
16	0.44	$Q-\parallel$ Mir	0.16	0.05	$Q-\perp$ Mir	0.15	$Q-\parallel$ Alf	
17	0.31	$Q-\parallel$ Mir	0.21	0.22	$Q-\perp$ Mir	0.42	$Q-\parallel$ Alf	$Q-\parallel$ Mir

$Q-\parallel$ corresponds to (\Leftrightarrow) $5^\circ < \theta_{kB} \lesssim 30^\circ$; $Q-\perp$ (\Leftrightarrow) $60^\circ \lesssim \theta_{kB} < 85^\circ$; MgS (\Leftrightarrow) Magnetosonic; Alf (\Leftrightarrow) Alfvén; IAc (\Leftrightarrow) Ion Acoustic; Mir (\Leftrightarrow) Mirror.

mate expression of our results. After listing the event number and value of C_B , Table 4d lists the best fitting mode (with the lowest deviation) along with the deviation D for that mode. The second best fitting mode is then listed with the difference between the deviation of the second best fitting mode (second lowest deviation) and the deviation of the best fitting mode. For all the events, the best fitting mode (lowest deviation) was

the mirror mode. The $Q-\perp$ mirror mode was the best fitting mode in 11 out of 17 events. The $Q-\parallel$ mirror mode was the best fitting mode in 6 of the 17 cases.

If the best fitting mode theoretical deviation was less than the difference between the deviation of the second best fitting mode and the deviation of the best fitting mode, we identified that mode as well identified in the last column of Table 4d. As can be seen from the table,

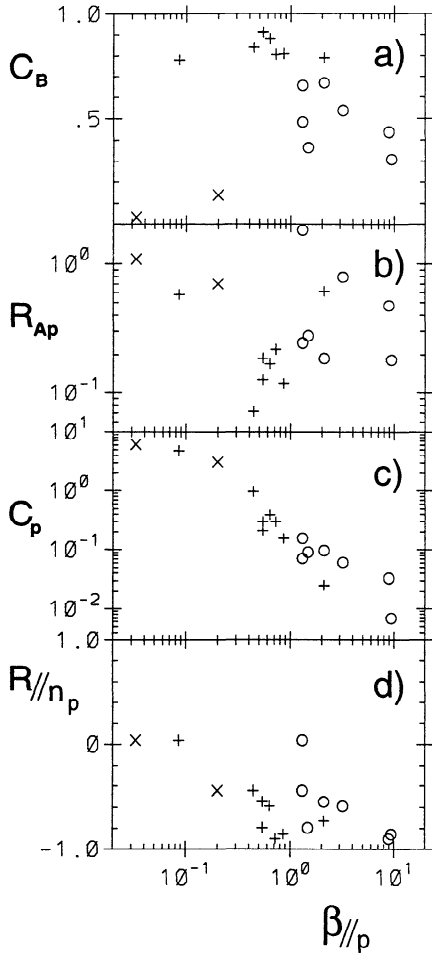


Figure 3. (a) C_B , (b) R_{Ap} , (c) C_p , and (d) $R_{\parallel n_p}$ plotted versus $\beta_{\parallel p}$ for the observed events. The plus (cross) is for $C_B \geq 0.75$ ($C_B \leq 0.25$); other events are plotted with a circle. There is a clear trend of C_p varying inversely with $\beta_{\parallel p}$.

only the mirror mode was well identified. The $Q-\perp$ mirror mode was well identified in 10 out of 17 events, while the $Q-\parallel$ mirror mode was well identified in 2 out of 17 events. Among the well-identified $Q-\perp$ mirror events was event 9, which was the example case with frequency-dependent spectra plotted in Figure 2. Despite the difference in method here (using a range of frequency rather than peak values, and using the Table 2 theoretical values rather than values found using the actual plasma parameters including a He^{2+} component), the deviations are almost the same (the deviation for the $Q-\perp$ mirror mode here is 0.07, whereas the value was 0.09 in Table 3). In Figure 4 we show the frequency-dependent spectra for event 3, for which the 0.01–0.04 Hz range was well identified as resulting from the $Q-\parallel$ mirror mode. In cases for which both the best fitting and second best fitting mode were the mirror mode, the third best fitting mode is listed along with the difference between the deviation of the third best fitting mode and the deviation of the best fitting mode.

Discussion

Linear theory predicts that the quasi-perpendicular mirror mode is the only unstable mode in this frequency range. Thus we have good reason to expect that the quasi-perpendicular mirror mode would be observed.

Theoretically, the quasi-parallel mirror mode has been described by Barnes [1966]. To our knowledge, this is the first time it has been identified observationally. For event 3 (well identified as the quasi-parallel mirror mode) we have done some additional analysis, which is described in Appendix C. If we associate the minimum variance direction with the wave vector and use the non-coplanar ratio R_{nc} as an independent transport ratio in the calculation of the mode deviation, then the identification as quasi-parallel mirror is no longer unique according to our criterion. This does introduce some doubt about the identification. However, due to the possible presence of multiple modes in the system (as indicated by the fact that there is not a single peak in frequency for the event), we consider the key assumption that the direction of \mathbf{k} be equivalent to the minimum variance direction to be questionable. Therefore we consider it most likely that our identification of the quasi-parallel mirror as based on the transport ratios is correct. If the identification is correct, we cannot explain generation of the quasi-parallel mirror mode using linear infinite homogeneous theory, since using that theory we find the mode to be heavily damped (see Table 2a). An explanation for generation of the quasi-parallel mirror mode would therefore have to involve the effects of inhomogeneity and nonlinearity. A recent hybrid simulation (N. Omidi and D. Winske, Structure of the magnetopause inferred from the kinetic Riemann problem, submitted to *Journal of Geophysical Research*, 1994) has demonstrated that quasi-perpendicular mirror waves from the magnetosheath can be compressed and amplified near the magnetopause, and makes clear the importance of nonlinear effects. But this simulation cannot address the possibility of quasi-parallel modes due to the one-dimensional nature of the simulation.

Because of the slow time resolution of the plasma instrument, we cannot use the transport ratios which use plasma fluctuations to check the identification of the higher-frequency waves which have been previously identified as ion cyclotron waves [Anderson et al., 1994]. Based on the good agreement of predicted and observed frequency range [Denton et al., 1994], the identification of these waves is probably correct. However, it is clear that $C_B \simeq 0$ (perpendicular fluctuations dominant) is not by itself adequate to distinguish ion cyclotron waves from the mirror mode since we have identified some waves as the $Q-\parallel$ mirror mode, which also has $C_B \simeq 0$.

Note added in proof: After the work described here was completed, it was pointed out (Paul Song, private communication, 1994) that the parallel phase ratio $R_{\parallel n_p}$ will not have a well defined value if C_B or C_p is very small; in such a case, the value of $R_{\parallel n_p}$ should not be used to identify the mode. In part, our method of writing the transport ratios with errors alleviates the prob-

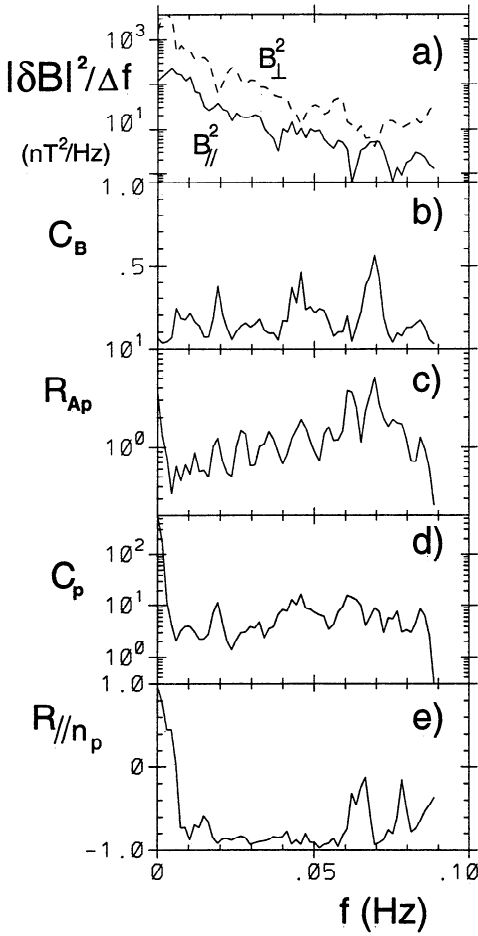


Figure 4. Same quantities as in Figure 2, but for the October 8, 1985, event (event 3 in Table 4a). $F_{cp} = 0.88$ Hz.

lem (with a large error, all the modes may have a theoretical value within the observed range of $R_{\parallel n_p}$, so that $R_{\parallel n_p}$ does not play a role in distinguishing the mode). However, in our analysis we have done some averaging which may have the effect of favoring theoretical modes with values of $R_{\parallel n_p}$ which are not extreme (values around 0 rather than at ± 1). Thus our procedure (using $R_{\parallel n_p}$ even when C_B or C_p is small) has favored the identification of the Alfvén and ion acoustic modes (which for $\beta_{\parallel p} \gtrsim 1$ have moderate values of $R_{\parallel n_p}$) over the mirror mode (which always has $R_{\parallel n_p} = -1$) and our conclusions remain valid.

Conclusions

We have summarized a group of five transport ratios that we believe are well suited for low-frequency ($f \ll F_{cp}$) mode identification. In Table 2 we have given detailed information on the theoretical values of these ratios for eight modes, the quasi-parallel and quasi-perpendicular magnetosonic, Alfvén, ion acoustic, and mirror modes. The dramatic dependence of C_p versus $\beta_{\parallel p}$ (Figure 3) for the observed waves shows that the data are as a whole consistent only with the mirror

mode. In order to get a more quantitative determination of the observed modes, we have defined a single parameter, the mode deviation D , which can be used as a measure of goodness-of-fit between the theoretical and observed transport ratios. Through use of the mode deviation we can find the mode which best describes the observed fluctuations; equally important, the mode deviation can be used to evaluate the uniqueness of a particular mode identification. Out of 17 time periods temporally close to a magnetopause crossing during which the IRM spacecraft observed waves, we find that 10 events have waves which are well identified as the $Q-\perp$ mirror mode, and two events have waves which are well identified as the $Q-\parallel$ mirror mode (at least when the noncoplanar ratio is not employed). In five of the events the waves were not well identified. The reason for the ambiguous cases may be the superposition of multiple modes, nonlinear effects, or random noise in the data.

Appendix A: Galilean Invariance of Transport Ratios

The constituents of our transport ratios, that is, the fluctuating magnetic field components, the fluctuating ion density and the fluctuating ion velocity, do not change under a Galilean velocity transformation. These constituents are independent of the observing frame by the following arguments. Magnetic field components are not invariant under a general relativistic Lorentz transformation, $\delta\mathbf{B}' \simeq \delta\mathbf{B} - \mathbf{v} \times \delta\mathbf{E}/c$. But the plasma flow speeds $v_0 \sim V_A$ of the magnetosheath are nonrelativistic; that is, $v_0/c \ll 1$. Using the Fourier-transformed Faraday's law ($|\delta\mathbf{E}|/|\delta\mathbf{B}| = \omega/kc$) and $\omega/k \lesssim V_A$, we have $\delta\mathbf{B}' \simeq \delta\mathbf{B}(1 - (V_A/c)^2(\omega/kV_A)) \sim \delta\mathbf{B}$ so the low-frequency fluctuations of concern do not vary under a Galilean transformation. Similarly, the invariance of a length measurement under a Galilean transformation implies that fluctuating densities do not change between the plasma and spacecraft frames. And, although the Doppler shift alters velocities measured from different frames, this shift is a constant which does not alter the fluctuating velocities that we utilize. The "Doppler ratio" of Song *et al.* [1994] is similar to our Alfvén ratio, but the Doppler ratio is dependent on the frame of reference through its dependence on v_0 and we will not make use of it.

Appendix B: Details of Plasma Model for Theoretical Calculation of Transport Ratios

In Table 3 we have calculated the theoretical transport ratios for the quasi-perpendicular mirror, ion acoustic, Alfvén, and magnetosonic modes using the measured ion density, temperature, and magnetic field strength averaged over the interval. Since IRM measures all ions together, we have assumed a population

of alpha particles according to the model described by Denton *et al.* [1994], which is based on measurements by AMPTE/Charge Composition Explorer. We assume therefore $n_\alpha/n_p = 0.04$, $T_{\perp\alpha}/T_{\perp p} = 5$, and $(T_\perp/T_\parallel)_\alpha = 1.3(T_\perp/T_\parallel)_p$. The value of $\beta_{\parallel p}$ was 0.86. For the mirror mode and quasi-perpendicular ion acoustic mode (the two best candidates for explaining the parallel fluctuations since $C_B \lesssim 1$ and $R_{\parallel n_p} < 0$), the magnetic fluctuations are in the plane of \mathbf{k} and \mathbf{B}_0 . With this assumption, we have from $\nabla \cdot \mathbf{B} = 0$, $\theta_{kB} = \tan^{-1}(\delta B_\parallel/\delta B_\perp)$ from which we get $\theta_{kB} \sim 70^\circ$ at the peak in parallel power of Figure 2. We assume for the finite frequency modes (ion acoustic, Alfvén, and magnetosonic) that the frequency in the plasma rest frame is the observed frequency. On the other hand, we assume for the mirror mode that the plasma is moving past the spacecraft at a speed equal to one half the Alfvén speed and that the observed frequency is due to the Doppler shift. The total range of θ_{kB} we consider is 60° to 80° , while we vary the rest frame frequency of the waves (k value for the mirror mode) by a factor of 2 up and down to account for varying Doppler shift.

Appendix C: Extra Analysis for Event 3

We have done some additional analysis for event 3. Using the minimum variance direction to infer the direction of the wave vector, we have calculated the value of the noncoplanar ratio R_{nc} , which is 0.46 for this event. Such a value would by itself favor identification with the quasi-parallel magnetosonic or Alfvén modes. Due to the poor agreement of other transport ratios for these modes, such an identification is still unlikely. However, if we use the noncoplanar ratio as a fifth transport ratio deviation D_{mt} and recalculate the total mode deviations, the event is no longer well identified as the quasi-parallel mirror mode according to our criterion for unique identification due to the fact that the total agreement with the quasi-parallel mirror mode is not so good as it was previously. The total deviation D for the quasi-parallel mirror mode would be 0.38 followed by 0.59 for the quasi-parallel ion acoustic mode and 0.62 for the quasi-perpendicular mirror mode. For the other modes the value of D is significantly higher. Identification of the minimum variance direction with the direction of \mathbf{k} would not be accurate if there are multiple modes in the plasma, so we consider the value of R_{nc} less reliable than the other transport ratios. For this reason we still consider it most likely that the identification as quasi-parallel mirror mode is correct. Note that the change in D for the quasi-parallel mirror mode made the mode identification nonunique not because of a low value of D for the quasi-parallel magnetosonic or Alfvén modes, but rather because with our definition of D , the quasi-parallel mirror mode became significantly large compared to the value for the quasi-parallel ion acoustic mode. The quasi-parallel ion acoustic mode should have a negligible value for R_{nc} just like the quasi-parallel mirror mode, and aside from the value of R_{nc} ,

the transport ratios for the quasi-parallel mirror mode were in far better agreement with the observed values than were those of the quasi-parallel ion acoustic mode.

We also did a higher order detuning of the data for event 3 and checked how the resulting fluctuating frequency varied with the plasma velocity. For this event the velocity dropped rapidly from 51 km/s in the first one sixth of the time period to 8 km/s or less in the rest of the time period. The wave frequency was found to be 0.029 in the first one sixth of the time segment and close to 0.018 for the rest of the time segment (though the errors were large enough that all the values could have been the same). If we assume that the component of the wave vector in the direction of plasma motion is constant, this result indicates some Doppler shift, but also that the mode has a finite frequency. (If there were zero real frequency in the plasma frame and therefore only a frequency due to Doppler shift, the frequency would be proportional to the plasma velocity if the assumption about the wave vector were correct.) One might consider this evidence against the mirror mode, but inhomogeneity does lead to a finite frequency for the mirror mode (Andrei Demekhov, personal communication, 1993).

Acknowledgments. We thank R. A. Treumann, P. Song and C.T. Russell for helpful discussions. We thank H. Lühr for providing us with AMPTE/IRM magnetic field data, and G. Paschmann for providing us with the IRM plasma data. This work has been supported with funding from NASA under grants NAG 5-1098 and NAGW-1652. X. Li acknowledges support from NSF ATM9221669. Work at Los Alamos was performed under the auspices of the U.S. Department of Energy (DOE) and was supported by the DOE Office of Basic Energy Sciences, Division of Engineering and Geosciences, and the SR&T Program of NASA. Work at the Johns Hopkins University Applied Physics Laboratory was supported by NASA, NSF, and ONR.

The Editor thanks D. Hubert and M.E. McKean for their assistance in evaluating this paper.

References

- Anderson, B.J., and S.A. Fuselier, Magnetic pulsations from 0.1 to 4.0 Hz and associated plasma properties in the Earth's subsolar magnetosheath and plasma depletion layer, *J. Geophys. Res.*, **98**, 1461, 1993.
- Anderson, B.J., S.A. Fuselier, and D. Murr, Electromagnetic ion cyclotron waves observed in the plasma depletion layer, *Geophys. Res. Lett.*, **18**, 1955, 1991.
- Anderson, B.J., S.A. Fuselier, S.P. Gary, and R.E. Denton, Magnetic spectral signatures in the Earth's magnetosheath and plasma depletion layer, *J. Geophys. Res.*, **99**, 5877, 1994.
- Barnes, A., Collisionless damping of hydromagnetic waves, *Phys. Fluids*, **9**, 1483, 1966.
- Belmont, G., D. Hubert, C. Lacombe, and F. Pantellini, Mirror mode and other compressive ULF modes, in *Proceedings of the 26th ESLAB Symposium*, Killarney, Ireland, 16-19 June 1992, *Eur. Space Agency Spec. Publ.*, *ESA SP-346*, 1992.
- Crooker, N.U., T.E. Eastman, and G.S. Stiles, Observations of plasma depletion in the magnetosheath at the dayside magnetopause, *J. Geophys. Res.*, **84**, 869, 1979.

- Denton, R.E., S.P. Gary, B.J. Anderson, S.A. Fuselier, and M.K. Hudson, Low-frequency magnetic fluctuation spectra in the magnetosheath and plasma depletion layer, *J. Geophys. Res.*, **99**, 5893, 1994.
- Engebretson, M.J., N. Lin, W. Baumjohann, H. Leuhr, B.J. Anderson, L.J. Zanetti, T.A. Potemra, R.L. McPherron, and M.G. Kivelson, A comparison of ULF fluctuations in the solar wind, magnetosheath, and dayside magnetosphere, I, Magnetosheath morphology, *J. Geophys. Res.*, **96**, 3441, 1991.
- Farris, M.H., C.T. Russell, and M.F. Thomsen, Magnetic structure of the low beta, quasi-perpendicular shock, *J. Geophys. Res.*, **98**, 15,285, 1993.
- Gary, S.P., Low-frequency waves in a high-beta collisionless plasma: polarization, compressibility and helicity, *J. Plasma Phys.*, **35**, 431, 1986.
- Gary, S.P., The mirror and ion cyclotron anisotropy instabilities, *J. Geophys. Res.*, **97**, 8519, 1992.
- Gary, S.P., and D. Winske, Correlation function ratios and the identification of space plasma instabilities, *J. Geophys. Res.*, **97**, 3103, 1992.
- Gary, S.P., and D. Winske, Simulations of ion cyclotron anisotropy instabilities in the terrestrial magnetosheath, *J. Geophys. Res.*, **98**, 9171, 1993.
- Gary, S.P., S.A. Fuselier, and B.J. Anderson, Ion anisotropy instabilities in the magnetosheath, *J. Geophys. Res.*, **98**, 1481, 1993.
- Gary, S.P., M.E. McKean, D. Winske, B.J. Anderson, R.E. Denton, and S.A. Fuselier, The proton cyclotron instability and the anisotropy/ β inverse correlation, *J. Geophys. Res.*, **99**, 5903, 1994.
- Gleaves, D.G., and D.J. Southwood, Magnetohydrodynamic fluctuations in the Earth's magnetosheath at 1500 LT: ISEE 1 and ISEE 2, *J. Geophys. Res.*, **96**, 129, 1991.
- Hubert, D., C. Perche, C.C. Harvey, C. Lacombe, and C.T. Russell, Observation of mirror waves downstream of a quasi-perpendicular shock, *Geophys. Res. Lett.*, **16**, 159, 1989a.
- Hubert, D., C.C. Harvey, and C.T. Russell, Observations of magnetohydrodynamic modes in the Earth's magnetosheath at 0600 LT, *J. Geophys. Res.*, **94**, 17,305, 1989b.
- Kaufmann, R.L., J.-T. Horng, and A. Wolfe, Large-amplitude hydromagnetic waves in the inner magnetosheath, *J. Geophys. Res.*, **75**, 4666, 1970.
- Krauss-Varban, D., N. Omidi, and K.B. Quest, Mode properties of low-frequency waves: Kinetic theory versus Hall-MHD, *J. Geophys. Res.*, **99**, 5987, 1994.
- Lacombe, C., E. Kinzelin, C.C. Harvey, D. Hubert, A. Mangeney, J. Elaoufir, D. Burgess, and C.T. Russell, Nature of the turbulence observed by ISEE 1-2 during a quasi-perpendicular crossing of the Earth's bow shock, *Ann. Geophys.*, **8**, 489, 1990.
- Lacombe, C., F.G.E. Pantellini, D. Hubert, C.C. Harvey, A. Mangeney, G. Belmont, and C.T. Russell, Mirror and Alfvénic waves observed by ISEE 1-2 during crossings of the Earth's bow shock, *Ann. Geophys.*, **10**, 772, 1992.
- Lühr, H., N. Klöcker, W. Oelschlägel, B. Hänsler, and M. Acuna, *IEEE Trans. Geosci. Remote Sens.*, **GE-23**, 259, 1985.
- Matthaeus, W.H., and M.L. Goldstein, Measurement of the rugged invariants of magnetohydrodynamic turbulence in the solar wind, *J. Geophys. Res.*, **87**, 6011, 1982.
- McKean, M.E., D. Winske, and S.P. Gary, Mirror and ion cyclotron anisotropy instabilities in the magnetosheath, *J. Geophys. Res.*, **97**, 19,421, 1992.
- Mousaizis, S., D. Hubert, A. Mangeney, C.C. Harvey, C. Perche, and C.T. Russell, Magnetohydrodynamic turbulence in the Earth magnetosheath, *Ann. Geophys.*, **4A**, 355, 1986.
- Orlowski, D.S., C.T. Russell, D. Krauss-Varban, and N. Omidi, A test of the Hall-MHD model: Application to low-frequency upstream waves at Venus, *J. Geophys. Res.*, **99**, 169, 1994.
- Paschmann, G., H. Loidl, P. Obermayer, M. Ertl, R. Laborenz, N. Sckopke, W. Baumjohann, C.W. Carlson, and D.W. Curtis, The plasma instrument for AMPTE IRM, *IEEE Trans. Geosci. Remote Sens.*, **GE-23**, 262, 1985.
- Paschmann, G., I. Papamastorakis, W. Baumjohann, N. Sckopke, C.W. Carlson, B.U.O. Sonnerup, and H. Lühr, The magnetopause for large magnetic shear: AMPTE/IRM observations, *J. Geophys. Res.*, **91**, 11,099, 1986.
- Sckopke, N., G. Paschmann, A.L. Brinca, C.W. Carlson, and H. Lühr, Ion thermalization in quasi-perpendicular shocks involving reflected ions, *J. Geophys. Res.*, **95**, 6337, 1990.
- Song, P., R.C. Elphic, C.T. Russell, J.T. Gosling, and C.A. Cattell, Structure and properties of the subsolar magnetopause for northward IMF: ISEE observations, *J. Geophys. Res.*, **95**, 6375, 1990.
- Song, P., C.T. Russell, and M.F. Thomsen, Waves in the inner magnetosheath: A case study, *Geophys. Res. Lett.*, **19**, 2191, 1992.
- Song, P., C.T. Russell, and C.Y. Huang, Wave properties near the subsolar magnetopause: Pc 1 waves in the sheath transition layer, *J. Geophys. Res.*, **98**, 5907, 1993.
- Song, P., C.T. Russell, and S.P. Gary, Identification of low-frequency fluctuations in the terrestrial magnetosheath, *J. Geophys. Res.*, **99**, 6011, 1994.
- Tajiri, M., Propagation of hydrodynamic waves in collisionless plasma, II, Kinetic approach, *J. Phys. Soc. Jpn.*, **22**, 1482, 1967.
- Tsurutani, B.T., E.J. Smith, R.R. Anderson, K.W. Ogilvie, J.D. Scudder, D.N. Baker, and S.J. Bame, Lion roars and nonoscillatory drift mirror waves in the magnetosheath, *J. Geophys. Res.*, **87**, 6060, 1982.

B.J. Anderson, Applied Physics Laboratory, Johns Hopkins University, Laurel, MD 20723-6099. (e-mail: Internet.anderson@ampvx2.jhuapl.edu)

R.E. Denton, J.W. LaBell, M. Lessard, and X. Li, Physics and Astronomy Department, Dartmouth College, 6127 Wilder Laboratory, Hanover, NH 03755-3528. (e-mail: Internet.richard.denton@dartmouth.edu; Internet.james.labelle@dartmouth.edu; Internet.marc.lessard@dartmouth.edu; Internet.xinlin.li@dartmouth.edu)

S.P. Gary, Los Alamos National Laboratory, Los Alamos, NM 87545. (e-mail: Internet.pgary@lanl.gov)

(Received July 13, 1994; revised November 16, 1994; accepted November 16, 1994.)